Bead magnetorelaxometry with an on-chip magnetoresistive sensor

Bjarke Thomas Dalslet,*[a] Christian Danvad Damsgaard,[a] Marco Donolato,[b] Maria Strømme,[c] Mattias Strömberg,[c] Peter Svedlindh[c] and Mikkel Fougt Hansen[a]

Received 6th May 2010, Accepted 9th September 2010
DOI: 10.1039/c0lc00002g

Magnetorelaxometry measurements on suspensions of magnetic beads are demonstrated using a planar Hall effect sensor chip embedded in a microfluidic system. The alternating magnetic field used for magnetizing the beads is provided by the sensor bias current and the complex magnetic susceptibility spectra are recorded as the 2nd harmonic of the sensor response. The complex magnetic susceptibility signal appears when a magnetic bead suspension is injected, it scales with the bead concentration, and it follows the Cole-Cole expression for Brownian relaxation. The complex magnetic susceptibility signal resembles that from conventional magnetorelaxometry done on the same samples apart from an offset in Brownian relaxation frequency. The time dependence of the signal can be rationalized as originating from sedimented beads.

1 Introduction

Brownian relaxation (BR) biodetection[1–8] is a method for detection of molecules where the target molecules attach to probe-functionalized magnetic beads and cause a detectable shift in the Brownian relaxation frequency of the beads. The BR approach allows volume based assays to be used and this may simplify the assay compared to substrate based methods. BR biodetection of several strains of bacteria has been demonstrated, such as *L. monocytogenes*, *V. vulnificus V. cholerae* and *E. coli*.[8,9] The spectrum of the magnetic susceptibility (the magnetorelaxometry spectrum) is used to measure the Brownian relaxation frequency and has hitherto been recorded using magnetometers based on induction coils[3–5] or Superconducting Quantum Interference Devices (SQUIDs)[6–8] in combination with alternating magnetic fields provided by external magnets. These setups are not ideally suited to the small sample volumes used in biosensing and are typically too expensive and bulky for point-of-care applications although miniaturization efforts are being made.[10]

On-chip magnetic biosensors relying on magnetic detection of magnetic beads can be developed as compact biosensors with a direct electrical readout (for reviews, see *e.g.*[11–15]). These sensors are sensitive to very small quantities of beads and the lower limit of sample volume is typically set by the delivering fluid system. This makes them suitable for lab-on-a-chip systems and other point-of-care applications. The magnetic bead detection is traditionally substrate based where beads are attached to the sensor surface by the target molecules. This requires biochemical patterning of the sensor surface to functionalize the sensitive areas and blocking of the remaining areas.

In this study we successfully demonstrate recording of magnetorelaxometry spectra using an on-chip planar Hall effect (PHE) magnetic field sensor integrated in a microfluidic system. The alternating magnetic field required for BR detection is provided by the sensor self-field due to the applied bias current and this removes the need for external magnets. To evaluate the validity of PHE magnetorelaxometry we compare it to magnetorelaxometry performed on the same bead batches in a conventional SQUID system and show the differences arising when using magnetic microsensors for detection. The results show that magnetic microsensors can potentially be used in volume based bioassays relying on changes in Brownian relaxation behavior of magnetic nanobeads in lab-on-a-chip systems. This is the first reported successful chip-based bead magnetorelaxometry study carried out at room temperature.

2 Theory

2.1 Sensor response

The magnetic response of an ensemble of magnetic particles in an oscillating magnetic field is described by the complex magnetic susceptibility

$$\chi = \chi' - i\chi'' = |\chi|\cos\phi - i|\chi|\sin\phi \quad (1)$$

where χ' and χ'' are the components of χ in-phase and out-of-phase with the magnetic field, respectively, and ϕ is the phase lag of the magnetic response with respect to the applied magnetic field.

The measurement geometry is illustrated in Fig. 1(a). The PHE sensor signal, V_y, can be written as

$$V_y = I_x[S_0\langle H_y\rangle + R_{\text{offset}}] \quad (2)$$

where I_x is the sensor current, S_0 is the sensitivity, $\langle H_y\rangle$ is the magnetic field averaged over the sensor surface and R_{offset} is the sensor offset.[16]

In these measurements, the beads are magnetized by the sensor self-field, H_s. Using that H_s is proportional to I_x and assuming that the bead magnetization is directly proportional to the

[a]*Department of Micro- and Nanotechnology, Technical University of Denmark, DTU Nanotech, Building 345 East, 2800 Kgs. Lyngby, Denmark*
[b]*LNESS Dipartimento di Fisica, Politecnico di Milano, Via Anzani 42, I-22100 Como, Italy*
[c]*Department of Engineering Sciences, The Ångström Laboratory, Box 534, SE-751 21 Uppsala, Sweden*

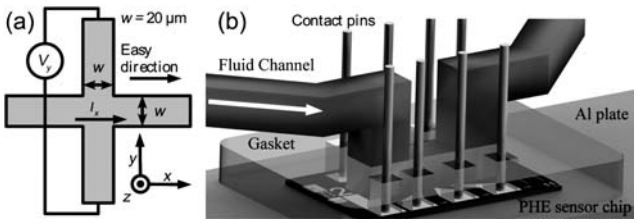

Fig. 1 (a) Sensor cross with definition of coordinate system and variables. (b) Illustration of the sensor chip mounted in the fluid system with integrated electrical contacts and temperature control. For clarity, the polycarbonate top is not shown, only fluid channel running inside it and the contact pins.

applied field, we can write the field from the beads averaged over the sensor surface, $\langle H_{\text{bead}} \rangle$, as

$$\langle H_{\text{bead}} \rangle = \gamma_1 \chi I_x \tag{3}$$

where χ is the bead susceptibility and γ_1 is a constant of proportionality depending on the sensor geometry and bead volume distribution.[17]

For our sensor design, about a tenth of the bias current is shunted through nonsensitive layers of the sensor. This gives rise to a finite average self-field, $\gamma_0 I_x$, acting on the sensitive layer, where γ_0 is a proportionality constant that depends on the geometry of the sensor and the resistance ratios between the sensitive layer and the other layers of the sensor stack.

With a current $I_x = I_{x,0}\sin(\omega t)$, where $I_{x,0}$ is the amplitude, $\omega = 2\pi f$ is the angular frequency and t is the time, $\langle H_y \rangle$ is

$$\langle H_y(t) \rangle = \gamma_0 I_{x,0}\sin(\omega t) + \gamma_1 I_{x,0}|\chi|\sin(\omega t - \phi) \tag{4}$$

Using the self-field to magnetize the beads ensures that only beads close to the sensor will be magnetized. Assuming a homogenous bead distribution about half of $\langle H_{\text{bead}} \rangle$ will arise from beads within 10 µm from the sensors of this study.[17] We will refer to this volume as the "sensitive volume".

In this study V_y is recorded using lock-in amplification tuned to the second harmonic of the current. The ideal second harmonic in-phase and out-of-phase signals V_2' and V_2'' are

$$V_2' = \frac{\sqrt{2}}{2\pi}\int_0^{2\pi} \sin(2\omega t) V_y(t) \mathrm{d}(\omega t) = -\frac{1}{2\sqrt{2}} I_{x,0}^2 S_0 \gamma_1 \chi'' \tag{5}$$

$$V_2'' = \frac{\sqrt{2}}{2\pi}\int_0^{2\pi} \sin\left(2\omega t + \frac{\pi}{2}\right) V_y(t) \mathrm{d}(\omega t) = -\frac{1}{2\sqrt{2}} I_{x,0}^2 S_0 (\gamma_0 + \gamma_1 \chi') \tag{6}$$

Thus, apart from the proportionality constant γ_1, χ'' and χ' can be extracted from V_2' and V_2'', respectively.

We note that any magnetic sensor with a signal that is linearly dependent on the field perpendicular to the bias current can be used instead of a PHE sensor. We use exchange-biased PHE sensors as these allow for a comparatively large I_x as well as a high sensitivity.[16]

2.2 Brownian relaxation

We consider the Brownian relaxation of magnetic beads, *i.e.*, a physical rotation of the bead in response to the applied magnetic field, which dominates Néel relaxation (superparamagnetic relaxation) in the investigated frequency window. The Brownian relaxation is characterized by the Brownian relaxation frequency f_B given by

$$f_B = \frac{k_B T}{6\pi\eta V_h} \tag{7}$$

where k_B is Boltzmann's constant, T is the absolute temperature, η is the dynamic viscosity of the fluid and V_h is the hydrodynamic volume of a bead. For a spherical particle this gives the hydrodynamic diameter $d_h = (6V_h/\pi)^{1/3}$, which is the diameter of an ideal hard sphere with relaxation properties identical to those of the measured bead. While d_h measured by Brownian relaxation is related to the real diameter of the bead, it depends on the stiffness, shape and axis of rotation of the bead and can thus be quite different. For a bead in a concentrated suspension d_h will also depend on bead agglomeration and, *e.g.*, magnetic, hydrodynamic, electrostatic and hydrophobic interactions between the beads and between the beads and the walls.

The relaxation behavior of an ensemble of beads with varying relaxation times can be described by the Cole-Cole equation for the complex susceptibility[18]

$$\chi = \chi' - \mathrm{i}\chi'' = \frac{\chi_0 - \chi_\infty}{1 + (\mathrm{i}f/f_B)^{1-\alpha}} + \chi_\infty \tag{8}$$

where α is the Cole-Cole parameter ($0 < \alpha < 1$), which equals zero for a single relaxation time (monodisperse sample) and is larger than zero for a distribution of relaxation times. χ_0 is the equilibrium susceptibility ($f = 0$) and χ_∞ is the susceptibility at $f = \infty$. The Cole-Cole equation yields a χ' spectrum that decreases from χ_0 at $f = 0$ to χ_∞ at $f = \infty$, and a χ'' spectrum with a peak at $f = f_B$. As the magnetic moment m of a sample is proportional to χ, eqn (8) equivalently describes the frequency dependence of the measured complex magnetization.

2.3 Bead sedimentation

The bead motion after injection can be estimated by a balance between drag, buoyancy and gravity forces, giving the vertical bead velocity

$$v_z = \frac{(\rho_f - \rho_b) d_b^2 g}{18\eta} \tag{9}$$

where ρ_f and ρ_b are the densities of the fluid and the beads, respectively, d_b is the bead diameter and g is the gravitational acceleration.

3 Experimental

3.1 Magnetic beads

The bead suspensions used were NH_2-terminated Nanomag-D 130 (labeled ND130) and Nanomag-D 250 (labeled ND250) from Micromod Partikeltechnologie GmbH, Rostock, Germany. The bead properties are summarized in Table 1. The bead stock suspensions with a concentration of 10 mg/mL were mixed

Table 1 Properties of the stock bead suspensions. d_b and ρ_b are the nominal diameter and density specified by the supplier, while the bead saturation specific magnetization, σ_s was measured in a commercial SQUID magnetometer

Label	d_b [nm]	ρ_b [kg/m^3]	σ_s [Am^2/kg]
ND130	130	3.0×10^3	51
ND250	250	2.5×10^3	74

with distilled and ultrasonically treated water to give the diluted bead suspensions used below. For the fluid system used in this study, where the channel height is 1 mm, insertion in eqn (9) gives sedimentation times of about 5 h for the ND250 suspension and 15 h for the ND130 suspension, respectively. Note, however, that the stability of bead suspensions is also sensitive to electrostatic and magnetic interactions between the beads and the sample history. For example, if the beads are electrically charged, the electrostatic repulsion can prevent or delay sedimentation. On the other hand, bead agglomerates will sediment faster than single beads.

3.2 SQUID experiments

SQUID experiments were conducted using a commercial SQUID magnetometer (MPMS-XL, Quantum Design) equipped with a μ-metal magnetic shield. A volume of 12.6 μl of each of the bead stock suspensions with a bead concentration of 10 mg/mL was put in a cylindrical Teflon sample container (1 mm liquid height). The magnetic shield was degaussed, the sample container was installed and the sample was centered in the SQUID. This was immediately followed by 11 and 12 consecutive recordings of the complex magnetic moment at 298 K (1000 to 3.7 Hz, 10 points per frequency decade, units of emu, excitation field of 160 A/m) for the ND130 and ND250 suspensions, respectively.

3.3 PHE sensor experiments

3.3.1 Sensor fabrication. The exchange-biased PHE sensors with the structure Si/SiO_2(800 nm)/Ta(5 nm)/$Ni_{81}Fe_{19}$ (30 nm)/$Mn_{76}Ir_{24}$ (20 nm)/Ta(5 nm) were deposited in a Kurt J. Lesker CMS-18 magnetron sputter system, and defined by lift-off. During deposition, a magnetic flux density of 20 mT was applied to define an easy magnetization direction of the sensitive $Ni_{81}Fe_{19}$ layer in the positive x-direction (see Fig. 1(a)). Gold contacts were deposited by e-beam evaporation and defined by lift-off. Subsequently, a 640 nm protective layer of SiO_2 was reactively sputter deposited through a shadow mask. The sensor cross had an active area of $w \times w = 20\ \mu m \times 20\ \mu m$ (fig. 1(a)). The sensitivity, S_0, for the sensor used in the experiments was found to -6.2×10^{-5} V m/A^2.

3.3.2 Sensor mounting and fluid system. The PHE chip was placed in a cavity in an Al plate with a Peltier PID temperature control ($\Delta T < 0.01$ K). On top of the chip was placed a polycarbonate top fabricated by micromilling with integrated fluid access channels and spring probes for electrical contacts. A polydimethylsiloxane gasket was pressed between the top and the chip defining a fluid channel of dimensions $l \times w \times h = 3$ mm $\times$ 0.4 mm $\times$ 1 mm. During experiments, a current I_x was applied through the sensors in the x -direction and the voltage drop V_y along the y -direction was measured as indicated for the sensor in Fig. 1(a). Fig. 1(b) shows a schematic of the system mounted in the experimental set-up with temperature control.

3.3.3 Measurement setup. An AC sensor bias current was supplied by a Keithley 6221 current source. After 100× amplification in a Stanford Research Systems (SRS) SR552 bipolar preamplifier, the sensor voltage signal V_y was extracted by use of a SRS SR830 lock-in amplifier and the second harmonic in-phase (V_2') and out-of-phase (V_2'') voltages were logged together with a timestamp and a temperature readout. During experiments, the sample holder temperature was kept constant at 298 K. All measurements were carried out without applied magnetic field and without electric or magnetic shielding.

3.3.4 Experimental procedure. A freshly mixed bead suspension of mass-to-volume concentration c was injected with a syringe. After injection, the inlet and outlet tubes were sealed with clamps. An AC current, $I_x = I_{x,0}\sin(2\pi ft)$, was turned on and f was repeatedly swept between 1 kHz and 1 Hz while recording V_2' and V_2''. Each sweep took about 40 min. Unless otherwise stated, an AC current amplitude of $I_{x,0} = 15$ mA was used. After a measurement series the sensor was flushed with water, dismounted, and gently wiped clean to remove remaining beads.

3.3.5 Data treatment and corrections. All recorded signals were divided by the SR552 preamplification factor. Fig. 2 illustrates the different data treatment steps used to obtain a corrected susceptibility spectrum for each sample.

A non-zero phase shift was measured even when no beads were present near the sensor (Fig. 2, spectrum (a)), *i.e.*, the signal had a frequency dependence. This phase shift was also observed when performing measurements of the voltage drop over a non-magnetic resistor and it can thus be attributed to the measurement setup. Spectrum (b) in Fig. 2 is obtained from spectrum (a) after a frequency dependent phase rotation: $V'_{2,b} = \cos(\phi_c)\cdot V'_{2,a} + \sin(\phi_c)\cdot V''_{2,a}$ and $V''_{2,b} = -\sin(\phi_c)\cdot V'_{2,a} + \cos(\phi_c)\cdot V''_{2,a}$, where the phase correction angle, ϕ_c, is chosen such that $V'_{2,b} = 0$. Note that for spectrum (b) $V''_{2,b}$ is independent of f indicating that the

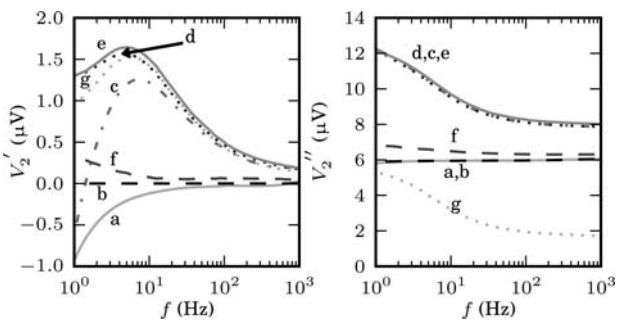

Fig. 2 Procedure for correcting measured V_2' and V_2'' spectra to obtain bead signals. a: Reference spectrum without beads. b: Phase corrected reference spectrum. c: Spectrum for the ND250 suspension $t = 2.7 \rightarrow 3.34$ h after injection. d: Spectrum c after phase correction. e: Time-interpolation of spectra to $t = 3.34$ h. f: Extrapolation of spectra to $t = 0$. g: Spectrum e after subtraction of spectrum f.

modulus of spectrum (a) is independent of f. To correct spectra with beads, we used ϕ_c found for a spectrum without beads. Spectra (c) and (d) in Fig. 2 show examples of frequency sweeps with magnetic beads before and after the phase correction, respectively.

Due to the measurement time of 40 min per spectrum a significant amount of beads sedimented during acquisition of a spectrum, and γ_1 therefore varied during a single frequency sweep. The low-frequency measurements were thus time offset from the high frequency measurements. Time normalized spectra (Fig. 2, spectrum (e)), where the signal for the entire spectrum was estimated for the same time, were linearly interpolated from consecutive spectra and used for analysis.

During injection the stray fields of the sensor and the field generated by the bias current acted as bead traps immediately trapping a significant number of beads on all edges of the $Ni_{81}Fe_{19}$ layer parallel to the y axis and along the central current line.[19] Beads trapped during injection were fixed in locations with large stray field gradients and these locations quickly saturated with beads. The strong trapping results in these beads having a Brownian relaxation frequency <1 Hz. The signal from these beads combined with the constant offset in V_2'' from the self-field was estimated by linear extrapolation to $t = 0$ (spectrum (f)). This signal was subtracted from all spectra to give the signal from non-trapped beads (spectrum (g)), which is the signal relevant for the Brownian relaxation measurements, and the signal presented in the results section.

4 Results

4.1 PHE signal time evolution

Fig. 3 shows V_2' and V_2'' as function of f measured after injection of 2 mg/mL ND250 suspension at time $t = 0$. A peak is visible at 5 Hz in the V_2' signal. The signal increases with time due to beads sedimenting into the sensitive volume.

The spectra can be fitted using Eq (8). After the final measurement the sensor was cleaned, and the spectrum was identical to that measured before bead injection, *i.e.* the corrected signal is zero. We thus conclude that the signal originates from the magnetic beads and that its frequency dependence can be attributed to Brownian relaxation.

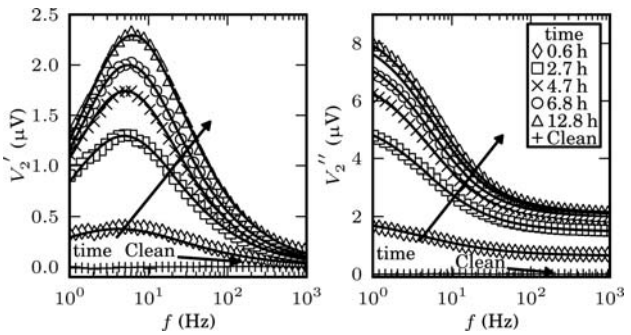

Fig. 3 Values of V_2' and V_2'' as function of frequency f and time t after injection of a 2 mg/mL ND250 suspension. The end time of each 40 min measurement is shown in the legend. Lines are fits to Eq (8). Also shown is the signal after sensor cleaning.

4.2 Bias current dependence

Eqs (5) and (6) predict that V_2' and V_2'' are proportional to $I_{x,0}^2$. Fig. 4 shows $V_2' \cdot I_{x,0}^{-2}$ and $V_2'' \cdot I_{x,0}^{-2}$ as function of f for the indicated values of $I_{x,0}$. As seen, the signals scale largely as predicted, although a small systematic increase in signal magnitude is seen for larger currents. This increase is too large to be attributed to Joule heating of the sensor, which would increase the sensor sensitivity,[20] but it could be caused by attraction of beads to the sensor area by the self-field.

4.3 Bead concentration dependence

Fig. 5 shows V_2' and V_2'' spectra measured 12–15 h after injection of ND250 suspensions with different bead concentrations. The signal intensity increases with the concentration, and the peak position is independent of the concentration. Fig. 5 also shows a spectrum measured on a ND130 suspension 12 h after injection. The signal intensity was still increasing at a steady rate when the spectrum was recorded. This spectrum fits poorly with Eq (8) at low frequencies, indicating a contribution from beads with very slow dynamics. The signal level of the 2 mg/ml ND130 suspension is 3–5 times lower than for the 2 mg/ml ND250 suspension even though the saturation magnetic moments of the two suspensions are comparable.

4.4 Comparison with SQUID measurements

Fig. 6(a) shows SQUID magnetorelaxometry measurements of the complex magnetization, $m = m' - im''$ recorded immediately after preparation of samples with a concentration of 10 mg/mL. The spectra correspond to d_h values of 111 nm and 330 nm and α values of 0.24 and 0.4 for the ND130 and ND250 suspensions, respectively.

Also shown in Fig. 6(a) are the corresponding spectra extracted from PHE sensor measurements of V_2' and V_2'' recorded 16 h (ND130) and 12 h (ND250) after injection of bead suspensions with a concentration of 2 mg/mL. The solid lines are fits to Eq (8). The spectra are consistent with Brownian relaxation as described by theory and correspond to hydrodynamic diameters of 196 nm and 420 nm for ND130 and ND250 suspensions, respectively.

Fig. 6(b) shows the time evolution of $\gamma_1(\chi_\infty - \chi_0)$ and f_B for ND130 and ND250 suspensions obtained from PHE sensor

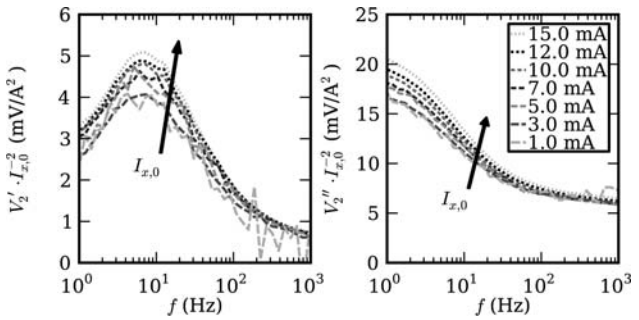

Fig. 4 Values of $V_2' \cdot I_{x,0}^{-2}$ and $V_2'' \cdot I_{x,0}^{-2}$ as function of frequency f and sensor bias current $I_{x,0}$ more than 23 h after injection of a 0.5 mg/mL ND250 suspension sample.

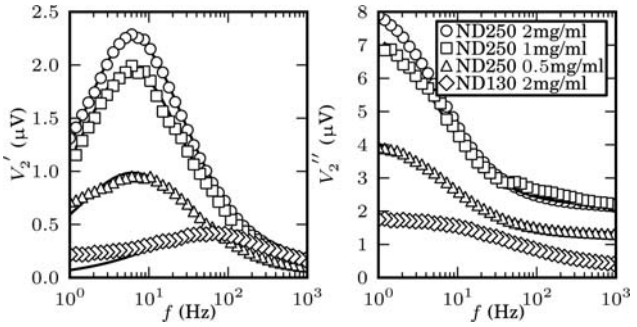

Fig. 5 Values of V_2' and V_2'' as function of frequency f for the indicated bead concentrations and bead sizes measured 12–15 h after injection of the bead suspensions. The lines are fits to Eq (8).

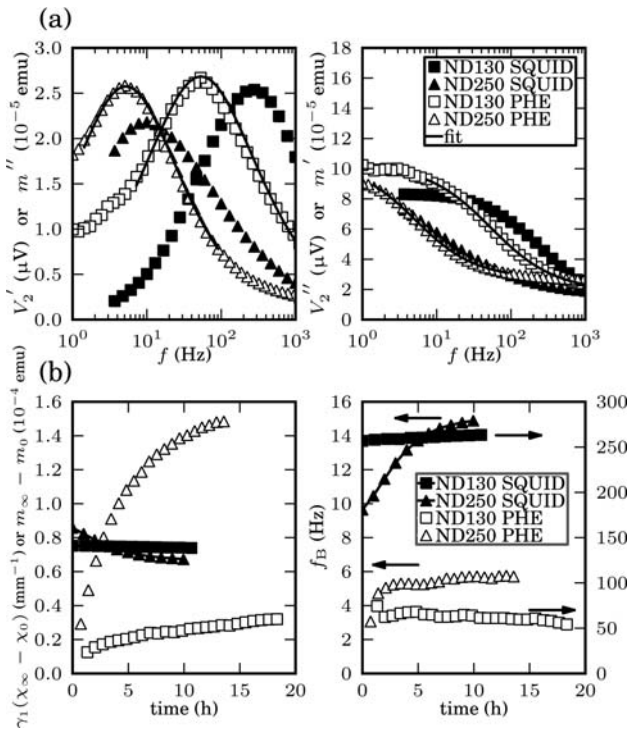

Fig. 6 (a) SQUID spectra of the complex magnetization $m = m' - im''$, on 10 mg/mL ND130 suspension and ND250 suspension and PHE spectra of V_2' and V_2'' obtained 12 h after injection of a 2 mg/mL ND250 suspension and 16 h after injection of a 2 mg/mL ND130 suspension. The lines are fits to Eq (8). The PHE spectrum for ND130 beads was multiplied by 5 for clarity. (b) Left: Values of $\gamma_1(\chi_\infty - \chi_0)$ obtained from fits of PHE measurements and $m_\infty - m_0$ obtained from SQUID measurements. Right: Values of f_B *vs.* time obtained from fits to SQUID and PHE measurements after injection or preparation of 2 mg/mL ND250 suspension (left axis) and ND130 (right axis).

measurements on bead suspensions with a concentration of 2 mg/mL. The figure also shows the values of $m_\infty - m_0$ obtained from SQUID measurements on bead suspensions with a concentration of 10 mg/mL. For PHE measurements on the ND250 suspension, $\gamma_1(\chi_\infty - \chi_0)$ initially increases steeply with time as beads move into the sensitive volume. After about 8 h the signal levels off and approaches steady state. For the same sample, the SQUID spectra show a decrease of $m_\infty - m_0$ with time. For the ND130 suspension the value of $\gamma_1(\chi_\infty - \chi_0)$ obtained from PHE measurements increases linearly with time and does not level off within the 18 h duration of the experiment. The values of $m_\infty - m_0$ obtained from SQUID measurements on the ND130 suspension are independent of time.

The values of f_B for $t < 2$ h extracted from PHE measurements are uncertain shortly after the bead suspension is injected due to the low signal and the measurement noise. For the ND250 suspension, the value of f_B is initially about 3 Hz but it stabilizes at about 6 Hz after several hours. For the ND130 suspension, the value of f_B extracted from PHE measurements is initially about 60 Hz but it decreases to about 50 Hz over several hours. The corresponding α-values obtained from fits to eqn (8) are stable for $t > 2$h at $\approx$0.25 (ND250) and $\approx$0.35 (ND130), respectively. The corresponding values of f_B extracted from SQUID measurements increase with time from 10 Hz to 15 Hz for the ND250 suspension before leveling off. For the ND130 suspension, f_B stays at 260 Hz.

5 Discussion

5.1 Overall interpretation

The values of d_h obtained by SQUID magnetorelaxometry measurements on ND130 and ND250 suspensions deviate from the nominal d_b values supplied by the bead manufacturer. As mentioned, this is likely due to batch to batch variations of the beads and interaction effects. To eliminate any influence from this we use the SQUID magnetorelaxometry measurements as the benchmark for evaluation PHE magnetorelaxometry rather than the nominal d_b values in the following.

As the results show, there are notable differences in the results obtained by SQUID and PHE magnetorelaxometry. These can to a large extent be explained by noting that the sensitive volumes of the two methods are different, and by keeping in mind that bead suspensions consist of a comparably wide range of bead sizes as reflected in the nonzero α values of the fits.

The SQUID magnetorelaxometry signal is due to rotating beads in the entire sample volume. Contact with the sample container can immobilize beads.[21] The magnitude of the SQUID signal thus decreases with time as sedimentation causes beads to stick to the container bottom. This effect is observed in Fig. 6(b) for the SQUID data obtained on the ND250 suspension. The magnitude of the signal for the ND130 suspension only changes little in the time window of the experiments due to the slower sedimentation of these beads.

By SQUID magnetorelaxometry it is found that the value of f_B increases with time as the larger beads and bead agglomerates sediment first and hence cease to contribute to the dynamic signal resulting in a decrease of the average value of V_h.[21]

The PHE magnetorelaxometry signal is due to magnetic beads in the small sensitive volume near the sensor surface. After injection of the bead suspension, the amount of beads in the sensitive volume increases with time due to sedimentation. Evidently, some of these beads remain able to rotate and hence the PHE signal increases with time as seen in Fig. 6(b).

By PHE magnetorelaxometry, much lower values of f_B are found than expected from the bead dimensions. Several factors can contribute to this: First, the larger beads sediment faster than

the smaller beads; therefore they will most likely contribute more to the signal than the smaller beads. Second, the beads contributing to the signal are in the vicinity of the sensor surface and also close to other beads. The interaction between the beads and between the beads and the sensor surface will increase the rotational friction of a single bead giving rise to a decrease of f_B. Moreover, when concentrated on the sensor surface, the beads are also more likely to form dimers or agglomerates, which also have a lower value of f_B. Finally, the magnetic field from the applied bias current is inhomogeneous, so the beads are affected by a magnetic force attracting them towards the sensor surface. This increases the rotational friction and also contributes to a lowering of f_B.

The two investigated bead types show different behavior. Values of $\gamma_1(\chi_\infty - \chi_0)$ recorded in the PHE measurements for the ND130 suspension are much smaller than those recorded for the ND250 suspension, and did not reach steady state in the time frame of our measurements. From the SQUID measurements on the same samples, we know that the total magnetic moment and the magnitudes of the magnetic susceptibility peaks of the ND130 and ND250 suspensions are comparable. Therefore, we conclude that beads in the ND130 suspension are entering the PHE sensitive volume more slowly than expected from the calculated 15 h sedimentation time. The slow sedimentation of beads in the ND130 suspension is also reflected in the nearly time independent SQUID spectra for these beads.

The discrepancy between the PHE data and the fits at low frequencies for the ND130 suspension in Fig. 6 is most likely due to bead agglomerates. The PHE measurements are more sensitive to agglomerates than SQUID measurements, where such a discrepancy is not seen, because agglomerates will sediment faster than single beads into the sensitive volume of the PHE sensor.

Agglomerates are likely also present in the ND250 suspension, but their expected BR frequency lies much lower than 1 Hz, which is the lower limit of our measurements.

5.2 Perspectives

PHE magnetorelaxometry presents itself as a viable alternative to traditional substrate based methods. An advantage of PHE magnetorelaxometry is that no biochemical functionalization of the sensor surface is necessary and hence this approach can be used for repeated measurements or continuous monitoring. Another benefit is that all sample treatment can be done before injection onto the chip, *i.e.*, no incubation step is needed after the sample has been injected. Finally, the molecules to be detected only need to attach to the beads instead of both the beads and the substrate.

PHE magnetorelaxometry differs from SQUID magnetorelaxometry in that it is mainly sensitive to beads in the sensitive volume near the sensor, whereas SQUID magnetorelaxometry is sensitive only to suspended beads. PHE magnetorelaxometry thus has a strong time dependence of the signal magnitude, it will measure lower Brownian relaxation frequencies and it is sensitive to bead trapping by the magnetic fields emanating from the sensor. The detailed mechanisms of the bead dynamics measured by PHE magnetorelaxometry are not understood and will be subject to further investigations. However, it should be noted that the experimental observations show a relaxation spectrum consistent with Brownian rotation dynamics as described by the Cole-Cole expression and that the values of f_B obtained from PHE magnetorelaxometry are at least as stable over time as those obtained by SQUID magnetorelaxometry. Furthermore, if the detection assay relies on heavy clustering of beads obtained, *e.g.*, by using rolling circle amplification (RCA) assays, these result in much larger frequency shifts than those observed between the SQUID and PHE measurements.[8]

The PHE magnetorelaxometry setup is much more compact than a SQUID setup, and it does not need external magnets or cooling of the sensor to cryogenic temperatures. This compactness allows it to be contained in a microfluidic system. Furthermore, it makes parallel analyses practical and make in situ reference measurements possible, which is an important criterion for realizing lab-on-a-chip systems. Finally, the small sensitive volume matches the requirement for small sample volumes found in lab-on-a-chip systems.

The setup used in this study was not optimized for magnetorelaxometry, and the influence of the set-up on the measurements and the requirement for signal corrections can likely be significantly reduced. Moreover, decreasing the fluid channel height would ensure that steady state could be reached much faster. Alternatively, applying an external magnetic field gradient could concentrate the beads in the sensitive volume of the sensor prior to measurements. Changing the sensor design may remove most of the stray fields ensuring a more homogenous bead coverage. In combination with better fluid injection, time normalization may be feasible for entirely removing the need to wait for a steady state.

6 Conclusions

We have shown that the complex magnetic susceptibility can be measured using on-chip magnetoresistive sensors operating at ambient conditions in a microfluidic system and have specifically demonstrated the feasibility of magnetorelaxometry measurements using a planar Hall effect sensor chip. The sensor self-field provided the alternating magnetic field removing the need for external magnets and there are no special requirements for magnetic shielding of the setup. Hence, the size of the complete sensor system is only limited by the electronics and equipment for the fluid handling. The measured dynamic magnetic signal can be interpreted as the complex magnetization due to Brownian relaxation of magnetic beads sedimenting on the sensor as (1) it appears when beads are inserted, (2) it scales with bead concentration, (3) it can be fitted with the Cole-Cole equation, (4) it increases in magnitude with time as beads sediment on the sensor, (5) it resembles SQUID magnetorelaxometry spectra apart from an offset in peak frequency.

The miniaturization and integration of dynamic magnetic measurements in a microfluidic channel demonstrated in the present study open new and unique opportunities for experiments on magnetic beads and particles in lab-on-a-chip systems. We have studied and highlighted the similarities and differences between on-chip and conventional magnetorelaxometry measurements that require further understanding and have to be carefully considered in biodetection experiments. The demonstration of in-channel volume-based biodetection by

magnetorelaxometry using magnetoresistive sensors is the topic of our ongoing work.

Acknowledgement

The Danish Council for Independent Research, Technology and Production Sciences (grant no. 09-062257), the Knut and Alice Wallenberg Foundation (KAW), the Swedish Foundation for Strategic Research (SSF), the Swedish Defense Nanotechnology program and the Swedish Research Council (VR) are gratefully acknowledged for their financial support.

References

1 J. Connolly and T. G. St Pierre, *J. Magn. Magn. Mater.*, 2001, **225**, 156–160.
2 R. Kötitz, W. Weitschies, L. Trahms, W. Brewer and W. Semmler, *J. Magn. Magn. Mater.*, 1999, **194**, 62–68.
3 A. P. Astalan, F. Ahrentorp, C. Johansson, K. Larsson and A. Krozer, *Biosens. Bioelectron.*, 2004, **19**, 945–951.
4 S.-H. Chung, A. Hoffmann, K. Guslienko, S. D. Bader, C. Liu, B. Kay, L. Makowski and L. Chen, *J. Appl. Phys.*, 2005, **97**, 10R101.
5 C.-Y. Hong, C. C. Wu, Y. C. Chiu, S. Y. Yang, H. E. Horng and H. C. Yang, *Appl. Phys. Lett.*, 2006, **88**, 212512.
6 F. Öisjöen, J. F. Schneiderman, M. Zaborowska, K. Shunmugavel, P. Magnelind, A. Kalaboukhov, K. Petersson, A. P. Astalan, C. Johansson and D. Winkler, *IEEE Trans. Appl. Supercond.*, 2009, **19**, 848.
7 K. Enpuku, H. Tokumitsu, Y. Sugimoto, H. Kuma, N. Hamasaki, A. Tsukamoto, T. Mizoguchi, A. Kandori, K. Yoshinaga, H. Kanzaki and N. Usuki, *IEEE Trans. Appl. Supercond.*, 2009, **19**, 844.
8 M. Strömberg, T. Z. G. Torre, J. Göransson, K. Gunnarsson, M. Nilsson, P. Svedlindh and M. Strømme, *Anal. Chem.*, 2009, **81**, 3398.
9 H. L. Grossman, W. R. Myers, V. J. Vreeland, R. Bruehl, M. D. Alper, C. R. Bertozzi and J. Clarke, *Proc. Natl. Acad. Sci. U. S. A.*, 2003, **101**, 129.
10 V. Schaller, A. Sanz-Velasco, A. Kalabukhov, J. F. Schneiderman, F. Öisjöen, A. Jesorka, A. P. Astalan, A. Krozer, C. Rusu, P. Enoksson and D. Winkler, *Lab Chip*, 2009, **9**, 3433–3436.
11 P. P. Freitas, R. Ferreira, S. Cardoso and F. Cardoso, *J. Phys.: Condens. Matter*, 2007, **19**, 165221.
12 D. L. Graham, H. A. Ferreira and P. P. Freitas, *Trends Biotechnol.*, 2004, **22**, 455.
13 M. Megens and M. Prins, *J. Magn. Magn. Mater.*, 2005, **293**, 702.
14 G. Reiss, H. Brueckl, A. Huetten, J. Schotter, M. Brzeska, M. Panhorst, D. S. A. Becker, P. B. Kamp, A. Puehler, K. Wojczykowski and P. Jutzi, *J. Mater. Res.*, 2005, **20**, 3294.
15 S. X. Wang and G. Li, *IEEE Trans. Magn.*, 2008, **44**, 1687.
16 C. D. Damsgaard, S. C. Freitas, P. P. Freitas and M. F. Hansen, *J. Appl. Phys.*, 2008, **103**, 07A302.
17 T. B. G. Hansen, C. D. Damsgaard, B. T. Dalslet and M. F. Hansen, *J. Appl. Phys.*, 2010, **107**(12), 124511.
18 K. S. Cole and R. H. Cole, *Chem. Phys.*, 1941, **9**, 341.
19 F. W. Østerberg, B. T. Dalslet, C. D. Damsgaard, S. C. Freitas, P. P. Freitas and M. F. Hansen, *IEEE Sens. J.*, 2009, **9**, 682.
20 C. D. Damsgaard, B. T. Dalslet, S. C. Freitas, P. P. Freitas and M. F. Hansen, *Sens. Actuators, A*, 2009, **156**, 103.
21 M. Strömberg, K. Gunnarsson, S. Valizadeh, P. Svedlindh and M. Strømme, *J. Appl. Phys.*, 2007, **101**, 023911.

